

Origin of the superconducting state in the collapsed tetragonal phase of KFe_2As_2

Daniel Guterding,* Steffen Backes, Harald O. Jeschke, and Roser Valentí
*Institut für Theoretische Physik, Goethe-Universität Frankfurt,
 Max-von-Laue-Straße 1, 60438 Frankfurt am Main, Germany*

Recently, KFe_2As_2 was shown to exhibit a structural phase transition from a tetragonal to a collapsed tetragonal phase under applied pressure of about 15 GPa. Surprisingly, the collapsed tetragonal phase hosts a superconducting state with $T_c \sim 12$ K, while the tetragonal phase is a $T_c \leq 3.4$ K superconductor. We show that the key difference between the previously known non-superconducting collapsed tetragonal phase in AFe_2As_2 (A= Ba, Ca, Eu, Sr) and the superconducting collapsed tetragonal phase in KFe_2As_2 is the qualitatively distinct electronic structure. While the collapsed phase in the former compounds features only electron pockets at the Brillouin zone boundary and no hole pockets are present in the Brillouin zone center, the collapsed phase in KFe_2As_2 has almost nested electron and hole pockets. Within a random phase approximation spin fluctuation approach we calculate the superconducting order parameter in the collapsed tetragonal phase. We propose that a Lifshitz transition associated with the structural collapse changes the pairing symmetry from d -wave (tetragonal) to s_{\pm} (collapsed tetragonal). Our DFT+DMFT calculations show that effects of correlations on the electronic structure of the collapsed tetragonal phase are minimal. Finally, we argue that our results are compatible with a change of sign of the Hall coefficient with pressure as observed experimentally.

PACS numbers: 71.15.Mb, 71.18.+y, 74.20.Pq, 74.70.Xa

The family of AFe_2As_2 (A= Ba, Ca, Eu, K, Sr) superconductors, also called 122 materials, has been intensively investigated in the past due to their richness in structural, magnetic and superconducting phases upon doping or application of pressure^{1–6}. One phase whose properties have been recently scrutinized at length is the collapsed tetragonal (CT) phase present in BaFe_2As_2 , CaFe_2As_2 , EuFe_2As_2 , and SrFe_2As_2 under pressure and in CaFe_2P_2 ^{7–14}. The structural collapse of this phase has been shown to be assisted by the formation of As $4p_z$ -As $4p_z$ bonds between adjacent Fe-As layers giving rise to a bonding-antibonding splitting of the As p_z bands¹⁵. It has been argued that this phase does not support superconductivity due to the absence of hole cylinders at the Brillouin zone center and the corresponding suppression of spin fluctuations^{10,16,17}. However, recently Ying *et al.*¹⁸ investigated the hole-doped end member of $\text{Ba}_{1-x}\text{K}_x\text{Fe}_2\text{As}_2$, KFe_2As_2 , under high pressure and observed a boost of the superconducting critical temperature T_c up to 12 K precisely when the system undergoes a structural phase transition to a CT phase at a pressure $P_c \sim 15$ GPa. These authors attributed this behavior to possible correlation effects. Moreover, measurements of the Hall coefficient showed a change from positive to negative sign upon pressure, indicating that the effective nature of charge carriers changes from holes to electrons with increasing pressure. Similar experiments are also reported in Ref. 19.

KFe_2As_2 has a few distinct features: at ambient pressure, the system shows superconductivity at $T_c = 3.4$ K and follows a V-shaped pressure dependence of T_c for moderate pressures with a local minimum at a pressure of 1.55 GPa²⁰. The origin of such behavior and the nature of the superconducting pairing symmetry are still under debate^{21–27}. However, it has been es-

tablished by a few experimental and theoretical investigations based on angle-resolved photoemission spectroscopy, de Haas-van Alphen measurements, and density functional theory combined with dynamical mean field theory (DFT+DMFT) calculations that correlation effects crucially influence the behavior of this system at

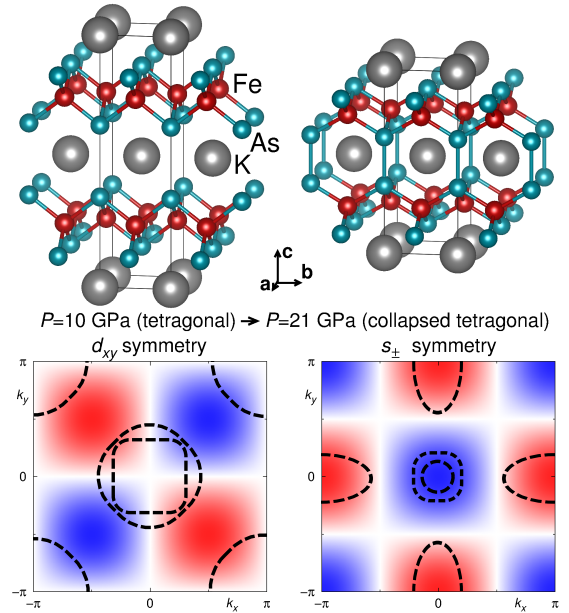


FIG. 1. (Color online) Crystal structure, schematic Fermi surface (dashed lines) and schematic superconducting gap function (background color) of KFe_2As_2 in the one-Fe Brillouin zone before and after the volume collapse. The Lifshitz transition associated with the formation of As $4p_z$ -As $4p_z$ bonds in the CT phase changes the superconducting pairing symmetry from d_{xy} to s_{\pm} .

$P = 0$ GPa^{28–35}. Application of pressure should nevertheless reduce the relative importance of correlations with respect to the bandwidth increase. In fact, recent DFT+DMFT studies on CaFe_2As_2 in the high-pressure CT phase show that the topology of the Fermi surface is basically unaffected by correlations^{36,37}. One could argue though, that at ambient pressure CaFe_2As_2 is less correlated than KFe_2As_2 and therefore, in KFe_2As_2 correlation effects may be still significant at finite pressure.

In order to resolve these questions, we performed density functional theory (DFT) as well as DFT+DMFT calculations for KFe_2As_2 in the CT phase. Our results show that the origin of superconductivity in the collapsed tetragonal phase in KFe_2As_2 lies in the qualitative changes in the electronic structure (Lifshitz transition) experienced under compression to a collapsed tetragonal phase and correlations play only a minor role. Whereas in the tetragonal phase at $P = 0$ GPa KFe_2As_2 features predominantly only hole pockets at the Brillouin zone center, at $P \sim 15$ GPa in the CT phase significant electron pockets emerge at the Brillouin zone boundary, which together with the hole pockets at the Brillouin zone center favor a superconducting state with s_{\pm} symmetry, as we show in our calculations of the superconducting gap function using the random phase approximation (RPA) spin fluctuation approach. Moreover, our results in the tetragonal phase of KFe_2As_2 at $P = 10$ GPa suggest a change of pairing symmetry from d_{xy} (tetragonal) to s_{\pm} upon entering the collapsed phase (see Fig. 1). This scenario is distinct from the physics of the CT phase in CaFe_2As_2 , where the hole pockets at the Brillouin zone center are absent. For comparison, we will present the susceptibility of collapsed tetragonal CaFe_2As_2 , which is representative for the collapsed phase of AFe_2As_2 (A = Ba, Ca, Eu, Sr). Our findings also suggest an explanation for the change of sign in the Hall coefficient upon entering the CT phase in KFe_2As_2 .

Density functional theory calculations were carried out using the all-electron full-potential local orbital (FPLO)³⁸ code. For the exchange-correlation functional we use the generalized gradient approximation (GGA) by Perdew, Burke, and Ernzerhof³⁹. All calculations were converged on $20 \times 20 \times 20$ k-point grids.

The structural parameters for the CT phase of KFe_2As_2 were taken from Ref. 18. We used the data points at $P \approx 21$ GPa, deep in the CT phase, where $a = 3.854$ Å and $c = 9.6$ Å. The fractional arsenic z -position ($z_{\text{As}} = 0.36795$) was determined *ab-initio* via structural relaxation using the FPLO code. We also performed calculations for the crystal structure of Ref. 19, where a preliminary experimental value for the arsenic z -position was given. The electronic structure is very similar to the one reported here. For the CT phase of CaFe_2As_2 we used experimental lattice parameters from Ref. 40 ($T = 40$ K, $P \approx 21$ GPa) and determined the fractional arsenic z -position ($z_{\text{As}} = 0.37045$) using FPLO. All Fe 3d orbitals are defined in a coordinate system rotated by 45° around the z -axis with respect to the

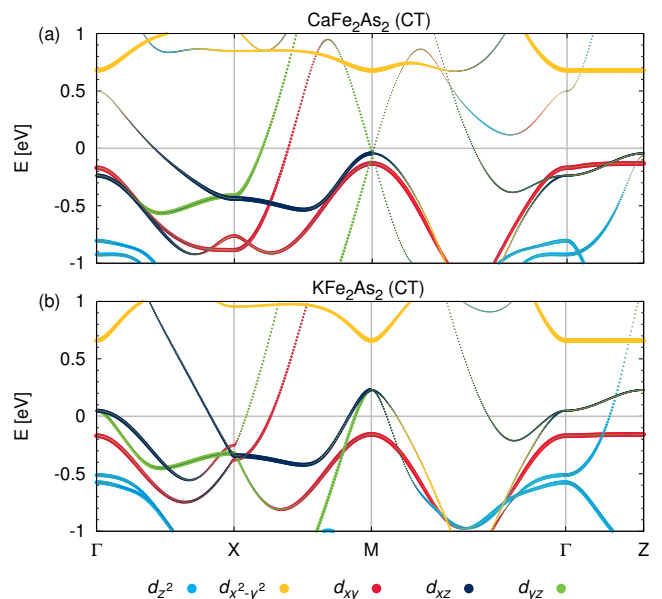


FIG. 2. (Color online) Electronic bandstructure of the collapsed tetragonal phase in (a) CaFe_2As_2 and (b) KFe_2As_2 . The path is chosen in the one-Fe equivalent Brillouin zone. The colors indicate the weights of Fe 3d states.

conventional $I4/mmm$ unit cell.

The electronic bandstructure in the collapsed tetragonal phase of CaFe_2As_2 and KFe_2As_2 is shown in Fig. 2. These results already reveal a striking difference between the CT phases of CaFe_2As_2 and KFe_2As_2 : while the former does not feature hole bands crossing the Fermi level at Γ and only one band crossing the Fermi level at M ($\pi, \pi, 0$), the latter does feature hole-pockets at both Γ and M in the one-Fe equivalent Brillouin zone. The reason for this difference in electronic structure is that KFe_2As_2 is strongly hole-doped compared to CaFe_2As_2 .

In Fig. 3 we show the Fermi surface in the one-Fe equivalent Brillouin zone at $k_z = 0$. In both cases, the Fermi surface is dominated by Fe $3d_{xz/yz}$ character. The hole cylinders in KFe_2As_2 span the entire k_z direction of the Brillouin zone, while only a small three-dimensional hole-pocket is present in CaFe_2As_2 (see Ref.⁴¹). For KFe_2As_2 , the hole-pockets at M ($\pi, \pi, 0$) and the electron pockets at X ($\pi, 0, 0$) are clearly nested, while no nesting is observed for CaFe_2As_2 . It is important to note here, that the folding vector in the 122 family of iron-based superconductors is (π, π, π) , so that the hole-pockets at M ($\pi, \pi, 0$) will be located at Z ($0, 0, \pi$) after unfolding the bands to the effective one-Fe picture⁴².

After qualitatively identifying the difference between the CT phases of CaFe_2As_2 and KFe_2As_2 , we calculate the non-interacting static susceptibility to verify that the better nesting of KFe_2As_2 generates stronger spin fluctuations. For that we constructed 16-band tight-binding models from the DFT results using projective Wannier functions as implemented in FPLO⁴³. We keep the Fe 3d and As 4p states, which corresponds to an energy win-

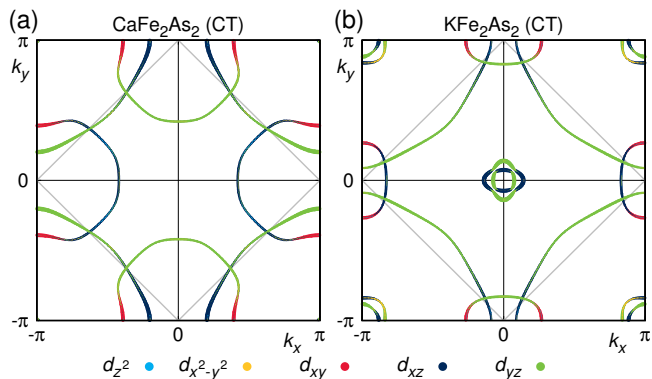


FIG. 3. (Color online) Fermi surface of the collapsed tetragonal phase in (a) CaFe_2As_2 and (b) KFe_2As_2 at $k_z = 0$. The full plot spans the one-Fe equivalent Brillouin zone, while the area enclosed by the grey lines is the two-Fe equivalent Brillouin zone. The colors indicate the weights of Fe 3d states.

dow from -7 eV to $+6$ eV. Subsequently, we unfold the 16-band model using our recently developed glide reflection unfolding technique⁴², which produces an effective eight-band model of the three-dimensional one-Fe Brillouin zone.

We analyse these eight-band models using the 3D version of random phase approximation (RPA) spin fluctuation theory⁴⁴ with a Hamiltonian $H = H_0 + H_{\text{int}}$, where H_0 is the eight-band tight-binding Hamiltonian derived from the *ab-initio* calculations, while H_{int} is the Hubbard-Hund interaction. The arsenic states are kept in the entire calculation, but interactions are considered only between Fe 3d states. Further information is given in Ref. 41.

The non-interacting static susceptibility in orbital-space is defined by Eq. (1), where matrix elements $a_\mu^s(\vec{k})$ resulting from the diagonalization of the initial Hamiltonian H_0 connect orbital and band-space denoted by indices s and μ respectively. The E_μ are the eigenvalues of H_0 and $f(E)$ is the Fermi function.

$$\chi_{st}^{pq}(\vec{q}) = -\frac{1}{N} \sum_{\vec{k}, \mu, \nu} a_\mu^s(\vec{k}) a_\mu^{p*}(\vec{k}) a_\nu^q(\vec{k} + \vec{q}) a_\nu^{t*}(\vec{k}) \times \frac{f(E_\nu(\vec{k} + \vec{q})) - f(E_\mu(\vec{k}))}{E_\nu(\vec{k} + \vec{q}) - E_\mu(\vec{k})} \quad (1)$$

The observable static susceptibility⁴¹ is defined as the sum over all elements χ_{aa}^{bb} of the full tensor $\chi(\vec{q}) = \frac{1}{2} \sum_{a,b} \chi_{aa}^{bb}(\vec{q})$.

The effective interaction in the singlet pairing channel is constructed from the static susceptibility tensor χ_{st}^{pq} which measures strength and wave-vector dependence of spin fluctuations, via the multiorbital RPA procedure. Both the original and effective interaction are discussed, e.g. in Ref. 45. We have shown previously that our implementation is capable of capturing effects of fine variations of shape and orbital character of the Fermi surface⁴⁶.

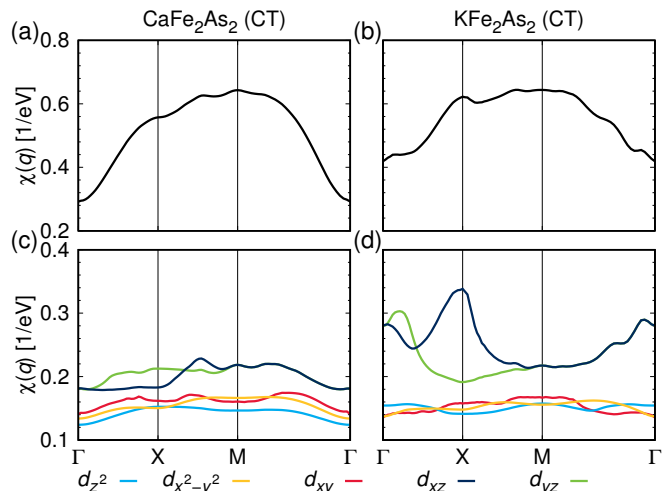


FIG. 4. (Color online) Summed static susceptibility (top) and its diagonal components χ_{aa}^{aa} (bottom) in the eight-band tight-binding model for [(a) and (c)] CaFe_2As_2 and [(b) and (d)] KFe_2As_2 in the one-Fe Brillouin zone. The colors identify the Fe 3d states.

At first glance, the observable static susceptibility displayed in Fig. 4 is comparable for CaFe_2As_2 and KFe_2As_2 . A key difference is however revealed upon investigation of the largest elements, i.e. the diagonal entries χ_{aa}^{aa} . These show that in CaFe_2As_2 the susceptibility has broad plateaus, while in KFe_2As_2 the susceptibility has a strong peak at X $(\pi, 0, 0)$ in the one-Fe Brillouin zone, which corresponds to the usual s_\pm pairing scenario that relies on electron-hole nesting. In CaFe_2As_2 the pairing interaction is highly frustrated because there is no clear peak in favor of one pairing channel.

We have also performed spin-polarized calculations for KFe_2As_2 at $P \approx 21$ GPa in order to confirm the antiferromagnetic instability we find in the linear response calculations. Out of ferromagnetic, Néel and stripe antiferromagnetic order only the stripe antiferromagnet is stable with small moments of $0.07\mu_B$ on Fe, in agreement with our calculations for the susceptibility.

The leading superconducting gap function of KFe_2As_2 in the CT phase is shown in Fig. 5. As expected from our susceptibility calculations, the pairing symmetry is s -wave with a sign-change between electron and hole-pockets. While the superconducting gap is nodeless in the $k_z = 0$ plane, the $k_z = \pi$ plane does show nodes where the orbital character changes from Fe $3d_{xz/yz}$ to Fe $3d_{xy}$. Note that this $k_z = \pi$ structure of the superconducting gap is exactly the same as in the well studied LaFeAsO compound⁴⁴, which shows that the CT phase of KFe_2As_2 closely resembles usual iron-based superconductors although it is much more three-dimensional than, e.g. in LaFeAsO .

We have also calculated the superconducting gap function for KFe_2As_2 at $P = 10$ GPa in the tetragonal phase and find d_{xy} as the leading pairing symmetry⁴¹. The dominant $d_{x^2-y^2}$ -solution obtained in model calculations

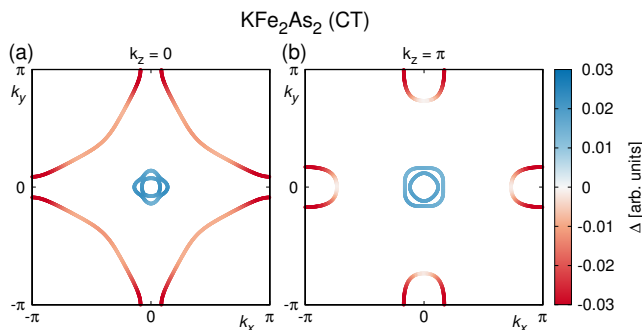


FIG. 5. (Color online) Leading superconducting gap function (s_{\pm}) of the eight-band model in the one-Fe Brillouin zone of KFe_2As_2 in the CT phase at (a) $k_z = 0$ and (b) $k_z = \pi$.

TABLE I. Mass renormalizations m^*/m_{LDA} of the Fe $3d$ orbitals in the collapsed tetragonal phase of KFe_2As_2 calculated with the LDA+DMFT method.

d_{z^2}	$d_{x^2-y^2}$	d_{xy}	$d_{xz/yz}$
1.318	1.309	1.319	1.445

based on rigid band shifts^{22,24} is also present in our calculation, but as a sub-leading solution. Our results strongly suggest that the Lifshitz transition, which occurs upon entering the collapsed tetragonal phase, changes the symmetry of the superconducting gap function from d -wave (tetragonal) to s -wave (CT) (see Fig. 1). The possible simultaneous change of pairing symmetry, density of states and T_c potentially opens up different routes to understanding their quantitative connection.

In order to estimate the strength of local electronic correlations in collapsed tetragonal KFe_2As_2 , we performed fully calculated self-consistent DFT+DMFT calculations. We used the same method as described in Ref. 35. The DFT calculation was performed by the WIEN2K⁴⁷ implementation of the full-potential linear augmented plane wave (FLAPW) method in the local density approximation (LDA) with 726 k -points in the irreducible Brillouin zone. We checked that the results of FPLO and WIEN2K agree on the DFT level. The Bloch wave functions are projected to the localized Fe $3d$ orbitals as described in Refs. 48 and 49. The energy window for projection was chosen from -7 to $+13$ eV, with the lower boundary lying in a gap in the density of states. For the solution of the DMFT impurity problem the continuous-time quantum Monte Carlo method in the hybridization expansion⁵⁰ as implemented in the ALPS^{51,52} project was employed (see Ref. 41 for more details). The mass-renormalizations are directly calculated from the analytically continued real part of the impurity self-energy $\Sigma(\omega)$

$$\text{via } \frac{m^*}{m_{\text{LDA}}} = 1 - \left. \frac{\partial \text{Re } \Sigma(\omega)}{\partial \omega} \right|_{\omega \rightarrow 0}.$$

Table I displays the orbital-resolved mass-renormalizations m^*/m_{LDA} for KFe_2As_2 in the collapsed tetragonal phase. The obtained values show that local electronic correlations in the CT phases of KFe_2As_2 and CaFe_2As_2 ^{36,37} are comparable. As in CaFe_2As_2 , the effects of local electronic correlations on the Fermi surface are negligible (see Ref. 41). The higher T_c of the collapsed phase in absence of strong correlations raises the question how important strong correlations are in general for iron-based superconductivity. This issue demands further investigation.

Finally, the change of dominant charge carriers from hole to electron-like states measured in the Hall-coefficient under pressure¹⁸ is naturally explained from our calculated Fermi surfaces. While KFe_2As_2 is known to show only hole-pockets at zero pressure, the CT phase features also large electron pockets. On a small fraction of these electron pockets, the dominating orbital character is Fe $3d_{xy}$ (Fig. 3). It was shown in Ref. 53 that quasiparticle lifetimes on the Fermi surface can be very anisotropic and long-lived states are favored where marginal orbital characters appear. As Fe $3d_{xy}$ character is only present on the electron pockets, these states contribute significantly to transport and are responsible for the negative sign of the Hall coefficient.

In summary, we have shown that the electronic structure of the collapsed tetragonal phase of KFe_2As_2 qualitatively differs from that of other known collapsed materials. Upon entering the CT phase, the Fermi surface of KFe_2As_2 undergoes a Lifshitz transition with electron pockets appearing at the Brillouin zone boundary, which are nested with the hole pockets at the Brillouin zone center. Thus, the spin fluctuations in collapsed tetragonal KFe_2As_2 resemble those of other iron-based superconductors in non-collapsed phases and the superconducting gap function assumes the well-known s_{\pm} symmetry. This is in contrast to other known materials in the CT phase, like CaFe_2As_2 , where hole pockets at the Brillouin zone center are absent and no superconductivity is favored. Based on our LDA+DMFT calculations, the CT phase of KFe_2As_2 is significantly less correlated than the tetragonal phase, and mass enhancements are comparable to the CT phase of CaFe_2As_2 . Finally, we suggest that the change of dominant charge carriers from hole to electron-like can be explained from anisotropic quasiparticle lifetimes.

ACKNOWLEDGMENTS

We thank the Deutsche Forschungsgemeinschaft for financial support through Grant No. SPP 1458.

* guterding@itp.uni-frankfurt.de

¹ M. Rotter, M. Tegel, and D. Johrendt, *Superconductivity at*

- 38 K in the Iron Arsenide $(\text{Ba}_{1-x}\text{K}_x)\text{Fe}_2\text{As}_2$, Phys. Rev. Lett. **101**, 107006 (2008).
- ² S. A. J. Kimber, A. Kreyssig, Y. Z. Zhang, H. O. Jeschke, R. Valentí, F. Yokaichiya, E. Colombier, J. Yan, T. C. Hansen, T. Chatterji, R. J. McQueeney, P. C. Canfield, A. I. Goldman, and D. N. Argyriou, *Similarities between structural distortions under pressure and chemical doping in superconducting BaFe_2As_2* , Nat. Mater. **8**, 471 (2009).
 - ³ J. Paglione and R. L. Greene, *High-temperature superconductivity in iron-based materials*, Nat. Phys. **6**, 645 (2010).
 - ⁴ E. Gati, S. Köhler, D. Guterding, B. Wolf, S. Knöner, S. Ran, S. L. Bud'ko, P. C. Canfield, and M. Lang, *Hydrostatic-pressure tuning of magnetic, nonmagnetic, and superconducting states in annealed $\text{Ca}(\text{Fe}_{1-x}\text{Co}_x)_2\text{As}_2$* , Phys. Rev. B **86**, 220511(R) (2012).
 - ⁵ S. Lee, J. Jiang, Y. Zhang, C.W. Bark, J. D. Weiss, C. Tarantini, C. T. Nelson, H.W. Jang, C. M. Folkman, S. H. Baek, A. Polyanskii, D. Abrahimov, A. Yamamoto, J.W. Park, X. Q. Pan, E. E. Hellstrom, D. C. Larbalestier, and C. B. Eom, *Template engineering of Co-doped BaFe_2As_2 single-crystal thin films*, Nat. Mater. **9**, 397 (2010).
 - ⁶ A. Leithe-Jasper, W. Schnelle, C. Geibel, and H. Rosner, *Superconducting State in $\text{SrFe}_{2-x}\text{Co}_x\text{As}_2$ by Internal Doping of the Iron Arsenide Layers*, Phys. Rev. Lett. **101**, 207004 (2008).
 - ⁷ W. Uhoya, A. Stemshorn, G. Tsoi, Y. K. Vohra, A. S. Sefat, B. C. Sales, K. M. Hope, and S. T. Weir, *Collapsed tetragonal phase and superconductivity of BaFe_2As_2 under high pressure*, Phys. Rev. B **82**, 144118 (2010).
 - ⁸ N. Ni, S. Nandi, A. Kreyssig, A. I. Goldman, E. D. Mun, S. L. Bud'ko, and P. C. Canfield, *First-order structural phase transition in CaFe_2As_2* , Phys. Rev. B **78**, 014523 (2008).
 - ⁹ Y.-Z. Zhang, H. C. Kandpal, I. Opahle, H. O. Jeschke, and R. Valentí, *Microscopic origin of pressure-induced phase transitions in the iron pnictide superconductors AFe_2As_2 : An ab initio molecular dynamics study*, Phys. Rev. B **80**, 094530 (2009).
 - ¹⁰ R. S. Dhaka, R. Jiang, S. Ran, S. L. Bud'ko, P. C. Canfield, B. N. Harmon, A. Kaminski, M. Tomic, R. Valentí, and Y. Lee *Dramatic changes in the electronic structure upon transition to the collapsed tetragonal phase in CaFe_2As_2* Phys. Rev. B **89**, 020511(R) (2014).
 - ¹¹ D. Kasinathan, M. Schmitt, K. Koepernik, A. Ormeci, K. Meier, U. Schwarz, M. Hanfland, C. Geibel, Y. Grin, A. Leithe-Jasper, and H. Rosner, *Symmetry-preserving lattice collapse in tetragonal $\text{SrFe}_{2-x}\text{Ru}_x\text{As}_2$ ($x=0,0.2$): A combined experimental and theoretical study*, Phys. Rev. B **84**, 054509 (2011).
 - ¹² W. Uhoya, G. Tsoi, Y. K. Vohra, M. A. McGuire, A. S. Sefat, B. C. Sales, D. Mandrus, and S. T. Weir, *Anomalous compressibility effects and superconductivity of EuFe_2As_2 under high pressures*, J. Phys.: Condens. Matter **22**, 292202 (2010).
 - ¹³ A. I. Coldea, C. M. J. Andrew, J. G. Analytis, R. D. McDonald, A. F. Bangura, J.-H. Chu, I. R. Fisher, and A. Carrington, *Topological Change of the Fermi Surface in Ternary Iron Pnictides with Reduced c/a Ratio: A de Haas-van Alphen Study of CaFe_2P_2* , Phys. Rev. Lett. **103**, 026404 (2009).
 - ¹⁴ N. Colonna, G. Profeta, A. Continenza, and S. Massidda, *Structural and magnetic properties of CaFe_2As_2 and BaFe_2As_2 from first-principles density functional theory*, Phys. Rev. B **83**, 094529 (2011).
 - ¹⁵ T. Yildirim, *Strong Coupling of the Fe-Spin State and the As-As Hybridization in Iron-Pnictide Superconductors from First-Principle Calculations*, Phys. Rev. Lett. **102**, 037003 (2009).
 - ¹⁶ D. K. Pratt, Y. Zhao, S. A. J. Kimber, A. Hiess, D. N. Argyriou, C. Broholm, A. Kreyssig, S. Nandi, S. L. Bud'ko, N. Ni, P. C. Canfield, R. J. McQueeney, and A. I. Goldman, *Suppression of antiferromagnetic spin fluctuations in the collapsed phase of CaFe_2As_2* , Phys. Rev. B **79**, 060510(R) (2009).
 - ¹⁷ J. H. Soh, G. S. Tucker, D. K. Pratt, D. L. Abernathy, M. B. Stone, S. Ran, S. L. Bud'ko, P. C. Canfield, A. Kreyssig, R. J. McQueeney, and A. I. Goldman, *Inelastic Neutron Scattering Study of a Nonmagnetic Collapsed Tetragonal Phase in Nonsuperconducting CaFe_2As_2 : Evidence of the Impact of Spin Fluctuations on Superconductivity in the Iron-Arsenide Compounds*, Phys. Rev. Lett. **111**, 227002 (2013).
 - ¹⁸ J.-J. Ying, L.-Y. Tang, V. V. Struzhkin, H.-K. Mao, A. G. Gavriluk, A.-F. Wang, X.-H. Chen, and X.-J. Chen, *Tripling the critical temperature of KFe_2As_2 by carrier switch*, arXiv:1501.00330 (unpublished).
 - ¹⁹ Y. Nakajima, R. Wang, T. Metz, X. Wang, L. Wang, H. Cynn, S. T. Weir, J. R. Jeffries, and J. Paglione, *High-temperature superconductivity stabilized by electron-hole interband coupling in collapsed tetragonal phase of KFe_2As_2 under high pressure*, Phys. Rev. B **91**, 060508(R) (2015).
 - ²⁰ F. F. Tafti, A. Juneau-Fecteau, M.-È. Delage, S. René de Cotret, J-Ph. Reid, A. F. Wang, X-G. Luo, X. H. Chen, N. Doiron-Leyraud, and L. Taillefer, *Sudden reversal in the pressure dependence of T_c in the iron-based superconductor KFe_2As_2* , Nat. Phys. **9**, 349 (2013).
 - ²¹ K. Okazaki, Y. Ota, Y. Kotani, W. Malaeb, Y. Ishida, T. Shimojima, T. Kiss, S. Watanabe, C-T. Chen, K. Kihou, C-H. Lee, A. Iyo, H. Eisaki, T. Saito, H. Fukazawa, Y. Kohori, K. Hashimoto, T. Shibauchi, Y. Matsuda, H. Ikeda, H. Miyahara, R. Arita, A. Chainani, and S. Shin, *Octet-Line Node Structure of Superconducting Order Parameter in KFe_2As_2* , Science **337**, 1314 (2012).
 - ²² R. Thomale, Ch. Platt, W. Hanke, J. Hu, and B. A. Bernevig, *Exotic d-Wave Superconducting State of Strongly Hole-Doped $\text{K}_x\text{Ba}_{1-x}\text{Fe}_2\text{As}_2$* , Phys. Rev. Lett. **107**, 117001 (2011).
 - ²³ J-Ph. Reid, M. A. Tanatar, A. Juneau-Fecteau, R. T. Gordon, S. René de Cotret, N. Doiron-Leyraud, T. Saito, H. Fukazawa, Y. Kohori, K. Kihou, C-H. Lee, A. Iyo, H. Eisaki, R. Prozorov, and L. Taillefer, *Universal Heat Conduction in the Iron Arsenide Superconductor KFe_2As_2 : Evidence of a d-Wave State*, Phys. Rev. Lett. **109**, 087001 (2012).
 - ²⁴ S. Maiti, M. M. Korshunov, T. A. Maier, P. J. Hirschfeld, and A. V. Chubukov, *Evolution of the Superconducting State of Fe-Based Compounds with Doping*, Phys. Rev. Lett. **107**, 147002 (2011).
 - ²⁵ K. Suzuki, H. Usui, and K. Kuroki, *Spin fluctuations and unconventional pairing in KFe_2As_2* , Phys. Rev. B **84**, 144514 (2011).
 - ²⁶ F. F. Tafti, J. P. Clancy, M. Lapointe-Major, C. Collignon, S. Faucher, J. A. Sears, A. Juneau-Fecteau, N. Doiron-Leyraud, A. F. Wang, X.-G. Luo, X. H. Chen, S. Desgreniers, Y.-J. Kim, and L. Taillefer, *Sudden reversal in the pressure dependence of T_c in the iron-based superconductor CsFe_2As_2 : A possible link between inelastic scattering*

- and pairing symmetry, Phys. Rev. B **89**, 134502 (2014).
- ²⁷ F. F. Tafti, A. Ouellet, A. Juneau-Fecteau, S. Faucher, M. Lapointe-Major, N. Doiron-Leyraud, A. F. Wang, X. G. Luo, X. H. Chen, and L. Taillefer, *Universal V-shaped temperature-pressure phase diagram in the iron-based superconductors KFe_2As_2 , $RbFe_2As_2$, and $CsFe_2As_2$* , Phys. Rev. B **91**, 054511 (2015).
- ²⁸ T. Terashima, M. Kimata, N. Kurita, H. Satsukawa, A. Harada, K. Hazama, M. Imai, A. Sato, K. Kihou, C-H. Lee, H. Kito, H. Eisaki, A. Iyo, T. Saito, H. Fukazawa, Y. Kohori, H. Harima, and S. Uji, *Fermi Surface and Mass Enhancements in KFe_2As_2 from de Haas-van Alphen Effect Measurements*, J. Phys. Soc. Jpn. **79**, 053702 (2010).
- ²⁹ T. Yoshida, I. Nishi, A. Fujimori, M. Yi, R. G. Moore, D-H. Lu, Z-X. Shen, K. Kihou, P. M. Shirage, H. Kito, C-H. Lee, A. Iyo, H. Eisaki, and H. Harima, *Fermi surfaces and quasi-particle band dispersions of the iron pnictide superconductor KFe_2As_2 observed by angle-resolved photoemission spectroscopy*, J. Phys. Chem. Solids **72**, 465 (2011).
- ³⁰ M. Kimata, T. Terashima, N. Kurita, H. Satsukawa, A. Harada, K. Kodama, K. Takehana, Y. Imanaka, T. Takamasu, K. Kihou, C-H. Lee, H. Kito, H. Eisaki, A. Iyo, H. Fukazawa, Y. Kohori, H. Harima, and S. Uji, *Cyclotron Resonance and Mass Enhancement by Electron Correlation in KFe_2As_2* , Phys. Rev. Lett. **107**, 166402 (2011).
- ³¹ T. Sato, N. Nakayama, Y. Sekiba, P. Richard, Y-M. Xu, S. Souma, T. Takahashi, G. F. Chen, J. L. Luo, N. L. Wang, and H. Ding, *Band Structure and Fermi Surface of an Extremely Overdoped Iron-Based Superconductor KFe_2As_2* , Phys. Rev. Lett. **103**, 047002 (2009).
- ³² T. Yoshida, S. Ideta, I. Nishi, A. Fujimori, M. Yi, R. G. Moore, S. K. Mo, D-H. Lu, Z-X. Shen, Z. Hussain, K. Kihou, P. M. Shirage, H. Kito, C-H. Lee, A. Iyo, H. Eisaki, and H. Harima, *Orbital character and electron correlation effects on two- and three-dimensional Fermi surfaces in KFe_2As_2 revealed by angle-resolved photoemission spectroscopy*, Front. Physics **2**, 17 (2014).
- ³³ T. Terashima, N. Kurita, M. Kimata, M. Tomita, S. Tsuchiya, M. Imai, A. Sato, K. Kihou, C-H. Lee, H. Kito, H. Eisaki, A. Iyo, T. Saito, H. Fukazawa, Y. Kohori, H. Harima, and S. Uji, *Fermi surface in KFe_2As_2 determined via de Haas-van Alphen oscillation measurements*, Phys. Rev. B **87**, 224512 (2013).
- ³⁴ Z. P. Yin, K. Haule, and G. Kotliar, *Kinetic frustration and the nature of the magnetic and paramagnetic states in iron pnictides and iron chalcogenides*, Nat. Mater. **10**, 932 (2011).
- ³⁵ S. Backes, D. Guterding, H. O. Jeschke, and R. Valentí, *Electronic structure and de Haas-van Alphen frequencies in KFe_2As_2 within LDA+DMFT*, New J. Phys. **16**, 085025 (2014).
- ³⁶ S. Mandal, R. E. Cohen, and K. Haule, *Pressure suppression of electron correlation in the collapsed tetragonal phase of $CaFe_2As_2$: A DFT-DMFT investigation*, Phys. Rev. B **90**, 060501(R) (2014).
- ³⁷ J. Diehl, S. Backes, D. Guterding, H. O. Jeschke, and R. Valentí, *Correlation effects in the tetragonal and collapsed tetragonal phase of $CaFe_2As_2$* , Phys. Rev. B **90**, 085110 (2014).
- ³⁸ K. Koepernik and H. Eschrig, *Full-potential nonorthogonal local-orbital minimum-basis band-structure scheme*, Phys. Rev. B **59**, 1743 (1999); <http://www.FPLO.de>
- ³⁹ J. P. Perdew, K. Burke, and M. Ernzerhof, *Generalized Gradient Approximation Made Simple*, Phys. Rev. Lett. **77**, 3865 (1996).
- ⁴⁰ R. Mittal, S. K. Mishra, S. L. Chaplot, S. V. Ovsyanikov, E. Greenberg, D. M. Trots, L. Dubrovinsky, Y. Su, Th. Bruckel, S. Matsuishi, H. Hosono, and G. Garbarino, *Ambient- and low-temperature synchrotron x-ray diffraction study of $BaFe_2As_2$ and $CaFe_2As_2$ at high pressures up to 56 GPa*, Phys. Rev. B **83**, 054503 (2011).
- ⁴¹ See Supplemental Material at [URL inserted by Publisher], which includes further information on the tight-binding model construction, the RPA pairing calculations, three-dimensional Fermi surface plots, an electronic structure calculation for a high-pressure non-collapsed structure of KFe_2As_2 and further details on the LDA+DMFT calculations outlined in the main text. For the latter we present momentum-resolved and momentum-integrated spectral functions and the Fermi surface.
- ⁴² M. Tomić, H. O. Jeschke, and R. Valentí, *Unfolding of electronic structure through induced representations of space groups: Application to Fe-based superconductors*, Phys. Rev. B **90**, 195121 (2014).
- ⁴³ H. Eschrig and K. Koepernik, *Tight-binding models for the iron-based superconductors*, Phys. Rev. B **80**, 104503 (2009).
- ⁴⁴ S. Graser, T. A. Maier, P. J. Hirschfeld, and D. J. Scalapino, *Near-degeneracy of several pairing channels in multiorbital models for the Fe pnictides*, New J. Phys. **11**, 025016 (2009).
- ⁴⁵ P. J. Hirschfeld, M. M. Korshunov, and I. I. Mazin, *Gap symmetry and structure of Fe-based superconductors*, Rep. Prog. Phys. **74**, 124508 (2011).
- ⁴⁶ D. Guterding, H. O. Jeschke, P. J. Hirschfeld, and R. Valentí, *Unified picture of the doping dependence of superconducting transition temperatures in alkali metal/ammonia intercalated FeSe*, Phys. Rev. B **91**, 041112(R) (2015).
- ⁴⁷ P. Blaha, K. Schwarz, G. K. H. Madsen, D. Kvasnicka, and J. Luitz, *An Augmented Plane Wave Plus Local Orbitals Program for Calculating Crystal Properties* (Karlheinz Schwarz, Techn. Universität Wien, Austria) (2001).
- ⁴⁸ M. Aichhorn, L. Pourovskii, V. Vildosola, M. Ferrero, O. Parcollet, T. Miyake, A. Georges, and S. Biermann, *Dynamical mean-field theory within an augmented plane-wave framework: Assessing electronic correlations in the iron pnictide $LaFeAsO$* , Phys. Rev. B **80**, 085101 (2009).
- ⁴⁹ J. Ferber, K. Foyevtsova, H. O. Jeschke, and R. Valentí, *Unveiling the microscopic nature of correlated organic conductors: The case of κ -(ET)₂Cu[N(CN)₂]Br_xCl_{1-x}*, Phys. Rev. B **89**, 205106 (2014).
- ⁵⁰ P. Werner, A. Comanac, L. de' Medici, M. Troyer, and A. J. Millis, *Continuous-Time Solver for Quantum Impurity Models*, Phys. Rev. Lett. **97**, 076405 (2006).
- ⁵¹ B. Bauer, L. D. Carr, H. G. Evertz, A. Feiguin, J. Freire, S. Fuchs, L. Gamper, J. Gukelberger, E. Gull, S. Guertler et al., *The ALPS project release 2.0: open source software for strongly correlated systems*, J. Stat. Mech. Theory Exp., P05001 (2011).
- ⁵² E. Gull, P. Werner, S. Fuchs, B. Surer, T. Pruschke, and M. Troyer, *Continuous-time quantum Monte Carlo impurity solvers*, Comput. Phys. Commun. **182**, 1078 (2011).
- ⁵³ A. F. Kemper, M. M. Korshunov, T. P. Devereaux, J. N. Fry, H-P. Cheng, and P. J. Hirschfeld, *Anisotropic quasi-particle lifetimes in Fe-based superconductors*, Phys. Rev. B **83**, 184516 (2011).

Origin of the superconducting state in the collapsed tetragonal phase of KFe_2As_2 : Supplemental Information

Daniel Guterding,* Steffen Backes, Harald O. Jeschke, and Roser Valentí
*Institut für Theoretische Physik, Goethe-Universität Frankfurt,
 Max-von-Laue-Straße 1, 60438 Frankfurt am Main, Germany*

I. DETAILS OF THE SUSCEPTIBILITY AND PAIRING CALCULATION

For calculating the susceptibility we used $30 \times 30 \times 10$ k-point grids and an inverse temperature of $\beta = 40 \text{ eV}^{-1}$. To calculate the pairing interaction, the susceptibility is needed at k-vectors that do in general not lie on a grid. Those susceptibility values are obtained using trilinear interpolation of the gridded data.

The pairing interaction is constructed using ~ 800 points on the three-dimensional Fermi surface. Consequently, the solution of the gap equation is available only on those points scattered in three-dimensional space. In order to obtain a graphical representation of the gap function on two-dimensional cuts through the Brillouin zone, we used multiscale radial basis function interpolation as implemented in ALGLIB (<http://www.alglib.net>).

The Hubbard-Hund interaction H_{int} includes the on-site intra (inter) orbital Coulomb interaction U (U'), the Hund's rule coupling J and the pair hopping energy J' . We assume spin rotation-invariant interaction parameters $U = 2.4 \text{ eV}$, $U' = U/2$, and $J = J' = U/4$. Because of the large bandwidth in the collapsed tetragonal phase, these comparatively large values are necessary to bring the system close to the RPA instability. Note however, that the symmetry of the superconducting gap in this system does not change, even if significantly reduced parameter values are considered.

The parameter values used in the RPA method are renormalized with respect to those in the DFT+DMFT method, because the electronic self-energy is neglected in the usual RPA scheme^{1,2}.

II. THREE DIMENSIONAL FERMI SURFACE

We extracted the three-dimensional Fermi surface of collapsed tetragonal CaFe_2As_2 and KFe_2As_2 from FPLO using $50 \times 50 \times 25$ k-point grids in the two-Fe equivalent Brillouin zone (Fig. 1). For CaFe_2As_2 only electron pockets in the Brillouin zone corners are observed. The three-dimensional hole pocket that arises from the bands at M ($\pi, \pi, 0$) is so small that it is not detected here with the given k-resolution. In KFe_2As_2 one of the hole cylinders is highly dispersive, while the central hole cylinder and the electron pockets located in the corners are nested throughout the entire Brillouin zone.

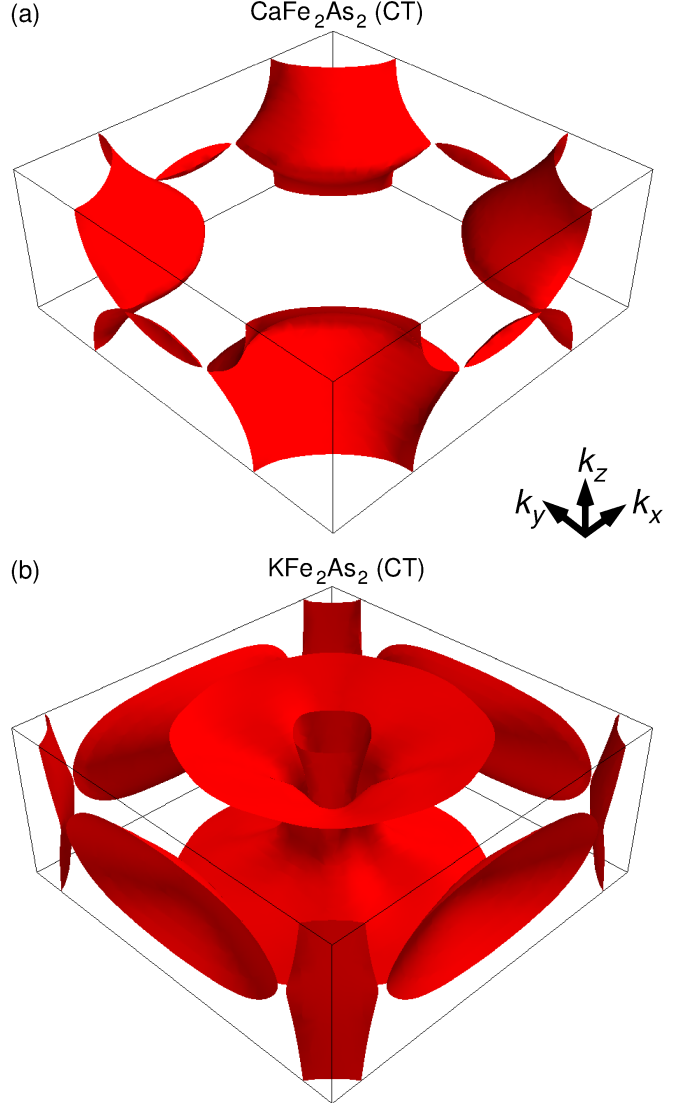


FIG. 1. Three-dimensional Fermi surface of (a) collapsed tetragonal CaFe_2As_2 and (b) collapsed tetragonal KFe_2As_2 (both at $P = 21 \text{ GPa}$) shown in the two-Fe equivalent Brillouin zone. The Γ -point is located in the center of the displayed volume.

III. DFT BANDSTRUCTURE AND FERMI SURFACE OF THE NON-COLLAPSED PHASE UNDER PRESSURE

To verify that electron pockets in KFe_2As_2 do not grow continuously with applied pressure, but rather appear as a

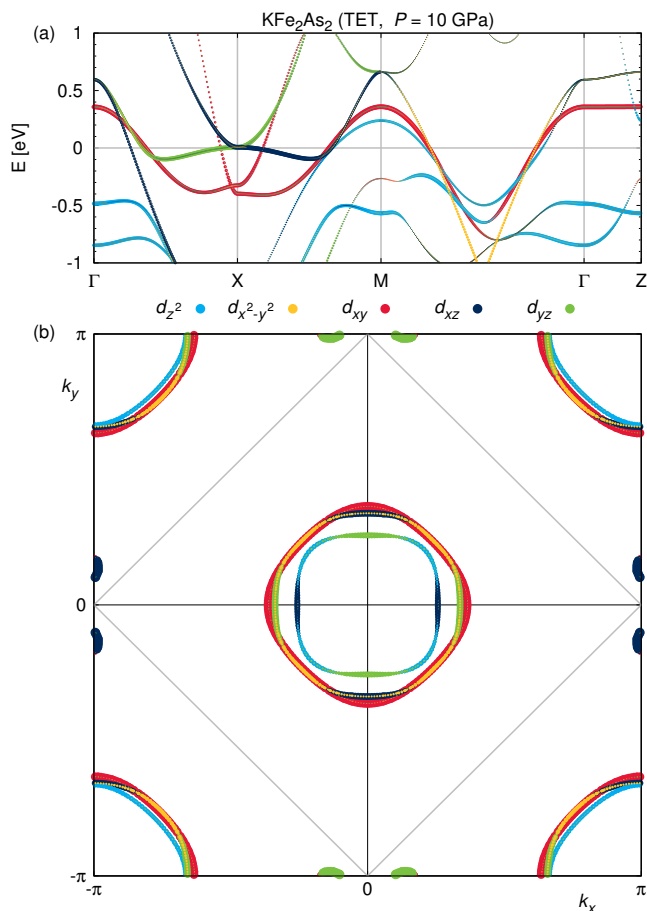


FIG. 2. (a) Electronic bandstructure in the one-Fe equivalent Brillouin zone and (b) Fermi surface of the $P \sim 10$ GPa non-collapsed tetragonal (TET) phase of KFe_2As_2 at $k_z = 0$. The full plot of the Fermi surface spans the one-Fe equivalent Brillouin zone, while the area enclosed by the grey lines is the two-Fe equivalent Brillouin zone. The colors indicate the weights of Fe 3d states.

result of the structural collapse, we have also prepared a crystal structure at $P \sim 10$ GPa, using the data from Ref. 3. The lattice parameters were chosen as $a = 3.663 \text{ \AA}$ and $c = 13.0 \text{ \AA}$. The fractional arsenic z -position ($z_{\text{As}} = 0.35750$) was again determined *ab-initio* via structural relaxation using the FPLO code.

No qualitative changes in the bandstructure and Fermi surface (Fig. 2) are observed compared to the ambient pressure structure⁴. Most importantly, electron pockets which are nested with the hole pockets in the Brillouin zone center are not present, even at high pressures slightly below the transition from the tetragonal to the collapsed tetragonal phase. We conclude that the appearance of electron pockets is directly linked to the structural collapse.

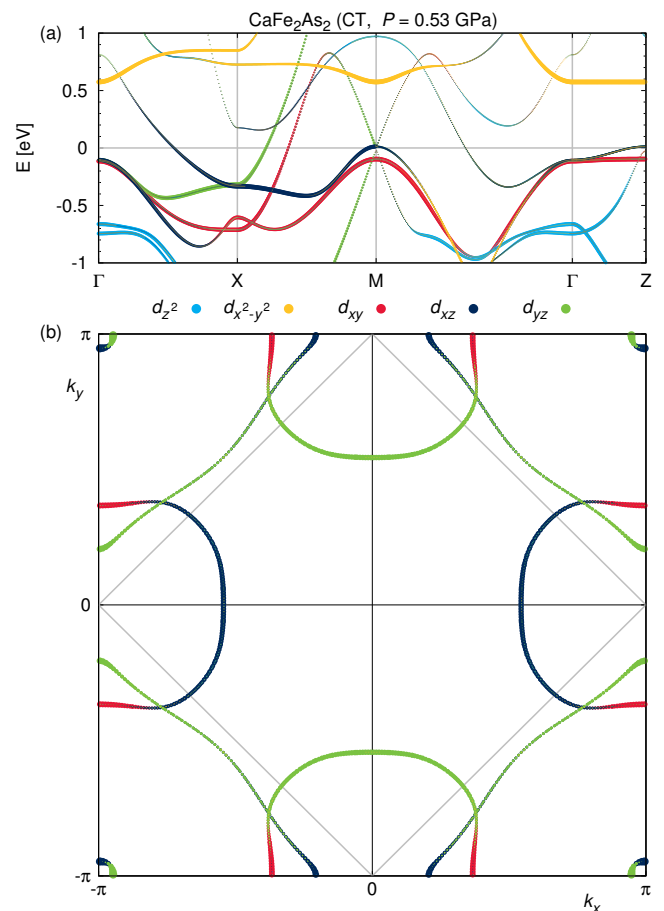


FIG. 3. (a) Electronic bandstructure in the one-Fe equivalent Brillouin zone and (b) Fermi surface of the $P = 0.53$ GPa collapsed tetragonal (CT) phase of CaFe_2As_2 at $k_z = 0$. The full plot of the Fermi surface spans the one-Fe equivalent Brillouin zone, while the area enclosed by the grey lines is the two-Fe equivalent Brillouin zone. The colors indicate the weights of Fe 3d states.

IV. BANDSTRUCTURE, FERMI SURFACE AND SUSCEPTIBILITY AT LOW PRESSURES

In the main paper we used crystal structures at $P = 21$ GPa for both materials of interest to ensure that results are comparable. Here we show the electronic bandstructure, Fermi surface and static susceptibility of CaFe_2As_2 at low pressure ($P = 0.53$ GPa), right after the structural collapse. We used the experimental structural parameters from Ref. 5, which are the same as in our previous GGA+DMFT study⁶. The differences compared to the high pressure results in the main text are purely quantitative.

The electronic bandstructure and Fermi surface are shown in Fig. 3. The static susceptibility is shown in Fig. 4. The overall enhancement of the susceptibility compared to the figures in the main text is a consequence of the smaller bandwidth at low pressure. The particular enhancement of the peak between X and M in the d_{xz} di-

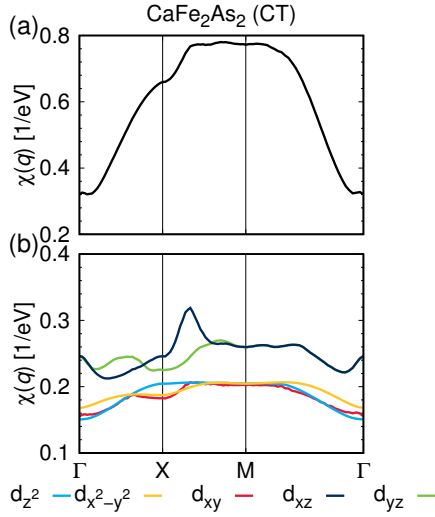


FIG. 4. Summed static susceptibility (a) and its diagonal components χ_{aa}^{aa} (b) in the eight-band tight-binding model for CaFe_2As_2 (CT, $P = 0.53$ GPa) in the one-Fe Brillouin zone. The colors identify the Fe 3d states.

agonal element of the susceptibility has its origin in the hole band crossing the Fermi level at the M point, which in turn contributes a small three-dimensional pocket.

V. DETAILS OF THE LDA+DMFT CALCULATION

For our DMFT calculations we used a temperature of 290 K, i.e. an inverse temperature $\beta = 40$ eV $^{-1}$. The interaction parameters are defined in terms of Slater integrals⁷ with an on-site Coulomb interaction $U = 4$ eV and Hund's rule coupling $J = 0.8$ eV. As the double counting correction we used the fully localized limit^{8,9} (FLL) scheme. Before the continuation of the imaginary-frequency self-energy to the real axis by stochastic analytic continuation¹⁰, the calculation was converged with 2×10^7 Monte-Carlo sweeps for the solution of the impurity model.

From the LDA+DMFT calculation we obtain the spectral function on real frequencies from the analytically continued self-energy as

$$A_{vv'}(k, \omega) = -\frac{1}{\pi} \Im \left[\frac{1}{(\omega + \mu)\delta_{vv'} - \epsilon_{vv'}(k) - \Sigma_{vv'}(k, \omega)} \right], \quad (1)$$

where μ is the chemical potential, $\epsilon_{vv'}(k) = \epsilon_v(k)\delta_{vv'}$ are the eigenenergies of the LDA Hamiltonian and $\Sigma_{vv'}(k, \omega)$ is the impurity self-energy upfolded to Bloch space by projectors $P_{mv}(k)$ (see Ref. 11 and 12)

$$\Sigma_{vv'}(k, \omega) = \sum_m P_{mv}^\dagger(k) (\Sigma_{mm}(\omega) - \Sigma_{DC}) P_{mv'}(k), \quad (2)$$

with the double-counting correction term Σ_{DC} taken in the fully-localized limit (FLL)^{8,9}. The diagonal entries

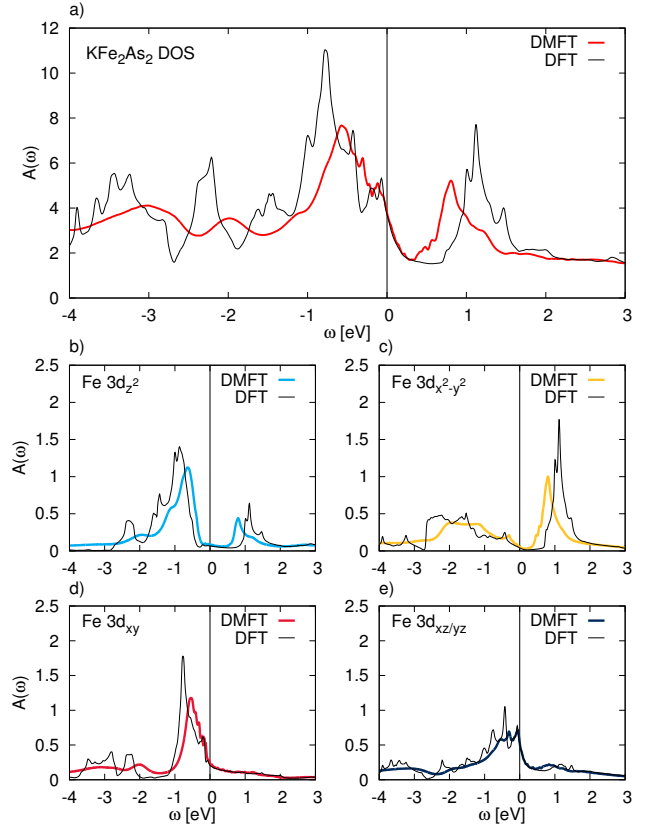


FIG. 5. The k-integrated spectral function (DOS) of KFe_2As_2 at $P = 21$ GPa as obtained within DFT compared to LDA+DMFT. The upper panel (a) shows the total DOS, with the DFT result (black line) and the renormalized LDA+DMFT result (red line). The lower four panels show the partial DOS of the Fe 3d orbitals: (b) $3d_{z^2}$, (c) $3d_{x^2-y^2}$, (d) $3d_{xy}$ and (e) $3d_{xz/yz}$ orbital.

of this object are then integrated over all bands v and k-points k to obtain the total density of states within LDA+DMFT shown in Fig. 5 (a). Additional projection onto the Fe 3d orbitals (denoted by index m) by

$$A_{mm'}(k, \omega) = -\frac{1}{\pi} \Im \left[\sum_{vv'} P_{mv}(k) \frac{1}{(\omega + \mu)\delta_{vv'} - \epsilon_{vv'}(k) - \Sigma_{vv'}(k, \omega)} P_{m'v'}^\dagger(k) \right], \quad (3)$$

is then used in the same fashion to obtain the orbital resolved density of states shown in Fig. 5 (b)-(e).

The k-resolved spectral function shown in Fig. 6 was obtained in the same manner, but only integrating over all bands v in order to keep the k-dependence. The orbital resolved Fermi surfaces shown in Fig. 7 and Fig. 8 were obtained by evaluating $A_{mm}(\omega)$ at the Fermi energy ($\omega = \omega_F$) on a 200×200 k-grid in the two-Fe Brillouin zone.

We observe moderate effects of renormalization and broadening in the density of states (see Fig. 5) with

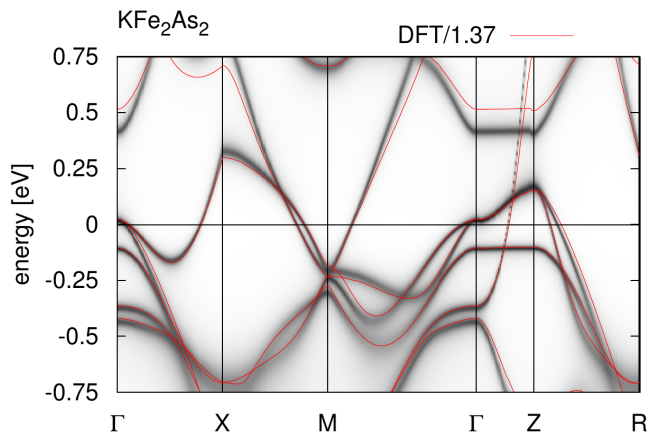


FIG. 6. The k-resolved spectral function of KFe_2As_2 at $P = 21$ GPa as obtained within LDA+DMFT. The red lines show the DFT bandstructure for comparison, rescaled by the average mass enhancement of 1.37. The labels on the x -axis correspond to high-symmetry points in the two-Fe Brillouin zone.

no significant change at the Fermi level. This is confirmed by the k -resolved spectral function (see Fig. 6). Using the FLL double-counting correction, we do not observe any topological changes in the Fermi surface, which closely resembles the DFT result (see Fig. 7 and Fig. 8). However, we observe a closing of the pockets at Γ when the nominal double-counting correction¹³ is considered. This indicates that the LDA+DMFT results slightly depend on the double-counting. Note that these changes do not affect our conclusions regarding the superconducting pairing symmetry since only a small fraction of the Brillouin zone around $k_z = 0$ is affected. As the relevant electron-hole nesting takes place around $k_z = \pi$, our superconducting pairing calculations based on the DFT bandstructure should be robust with respect to the effects of correlations.

Note that the Fermi surface plots (Fig. 7 and Fig. 8) have to be rotated by 45° in the plane in order to compare with the Fermi surface plots in the original paper. In 122 compounds the Z-point of the two-Fe Brillouin zone corresponds to the M-point of the one-Fe Brillouin zone.

* guterding@itp.uni-frankfurt.de

- ¹ S. Graser, T. A. Maier, P. J. Hirschfeld, and D. J. Scalapino, *Near-degeneracy of several pairing channels in multiorbital models for the Fe pnictides*, New J. Phys. **11**, 025016 (2009).
- ² K. Kuroki, H. Usui, S. Onari, R. Arita, and H. Aoki, *Pnictogen height as a possible switch between high- T_c nodeless and low- T_c nodal pairings in the iron-based superconductors*, Phys. Rev. B **79**, 224511 (2009).
- ³ J.-J. Ying, L.-Y. Tang, V. V. Struzhkin, H.-K. Mao, A. G. Gavriluk, A.-F. Wang, X.-H. Chen, and X.-J. Chen, *Tripling the critical temperature of KFe_2As_2 by carrier switch*, arXiv:1501.00330 (unpublished).
- ⁴ S. Backes, D. Guterding, H. O. Jeschke, and R. Valentí, *Electronic structure and de Haas-van Alphen frequencies in KFe_2As_2 within LDA+DMFT*, New J. Phys. **16**, 085025 (2014).
- ⁵ A. Kreyssig, M. A. Green, Y. Lee, G. D. Samolyuk, P. Zajdel, J. W. Lynn, S. L. Bud'ko, M. S. Torikachvili, N. Ni, S. Nandi *et al.*, *Pressure-induced volume-collapsed tetragonal phase of CaFe_2As_2 as seen via neutron scattering*, Phys. Rev. B **78**, 184517 (2008).
- ⁶ J. Diehl, S. Backes, D. Guterding, H. O. Jeschke, and R. Valentí, *Correlation effects in the tetragonal and collapsed tetragonal phase of CaFe_2As_2* , Phys. Rev. B **90**, 085110 (2014).

- ⁷ A. I. Liechtenstein, V. I. Anisimov, and J. Zaanen, *Density-functional theory and strong interactions: Orbital ordering in Mott-Hubbard insulators*, Phys. Rev. B **52**, R5467(R) (1995).
- ⁸ S. L. Dudarev, G. A. Botton, S. Y. Savrasov, C. J. Humphreys, and A. P. Sutton, *Electron-energy-loss spectra and the structural stability of nickel oxide: An LSDA+ U study*, Phys. Rev. B **57**, 1505 (1998).
- ⁹ V. I. Anisimov, I. V. Solovyev, M. A. Korotin, M. T. Czyzyk, and G. A. Sawatzky, *Density-functional theory and NiO photoemission spectra*, Phys. Rev. B **48**, 16929 (1993).
- ¹⁰ K. S. D. Beach, *Identifying the maximum entropy method as a special limit of stochastic analytic continuation*, arXiv:cond-mat/0403055 (unpublished) (2004).
- ¹¹ M. Aichhorn, L. Pourovskii, V. Vildosola, M. Ferrero, O. Parcollet, T. Miyake, A. Georges, and S. Biermann, *Dynamical mean-field theory within an augmented plane-wave framework: Assessing electronic correlations in the iron pnictide LaFeAsO* , Phys. Rev. B **80**, 085101 (2009).
- ¹² J. Ferber, K. Foyevtsova, H. O. Jeschke, and R. Valentí, *Unveiling the microscopic nature of correlated organic conductors: The case of κ -(ET)₂ $\text{Cu}[\text{N}(\text{CN})_2]\text{Br}_x\text{Cl}_{1-x}$* , Phys. Rev. B **89**, 205106 (2014).
- ¹³ K. Haule, *Exact double-counting in combining the Dynamical Mean Field Theory and the Density Functional Theory*, arXiv:1501.03438 (unpublished).

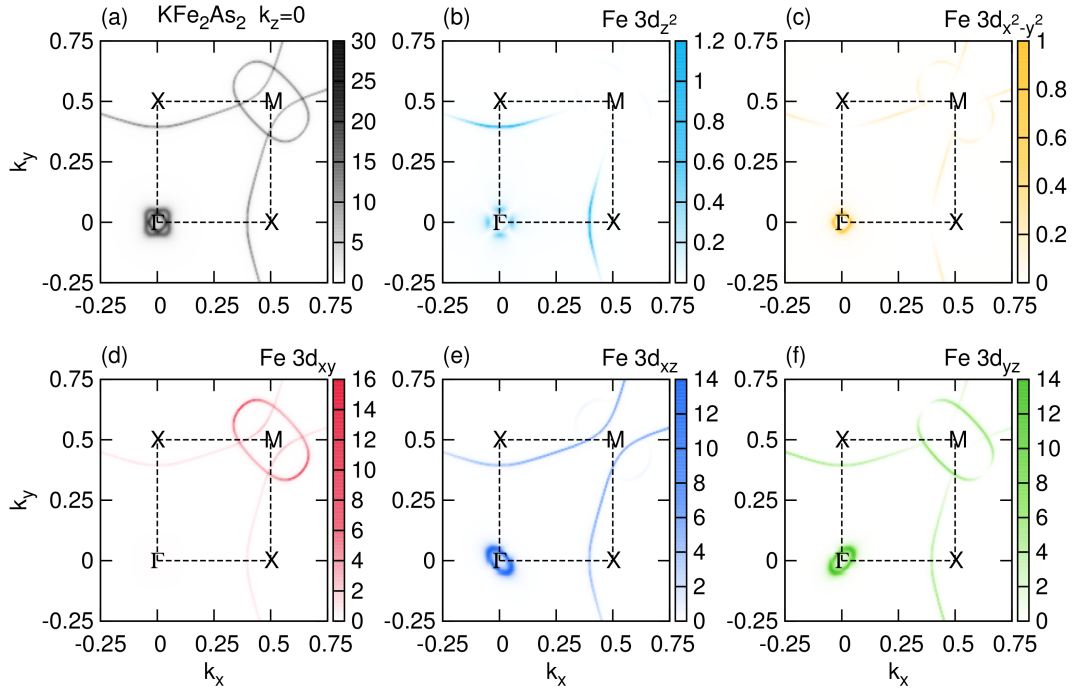


FIG. 7. The $k_z = 0$ Fermi surface of KFe_2As_2 at $P = 21$ GPa as obtained within LDA+DMFT in the two-Fe Brillouin zone. Panel (a) shows the total spectral function, while panels (b)-(f) show the orbital resolved spectral function for the Fe $3d$ orbitals.

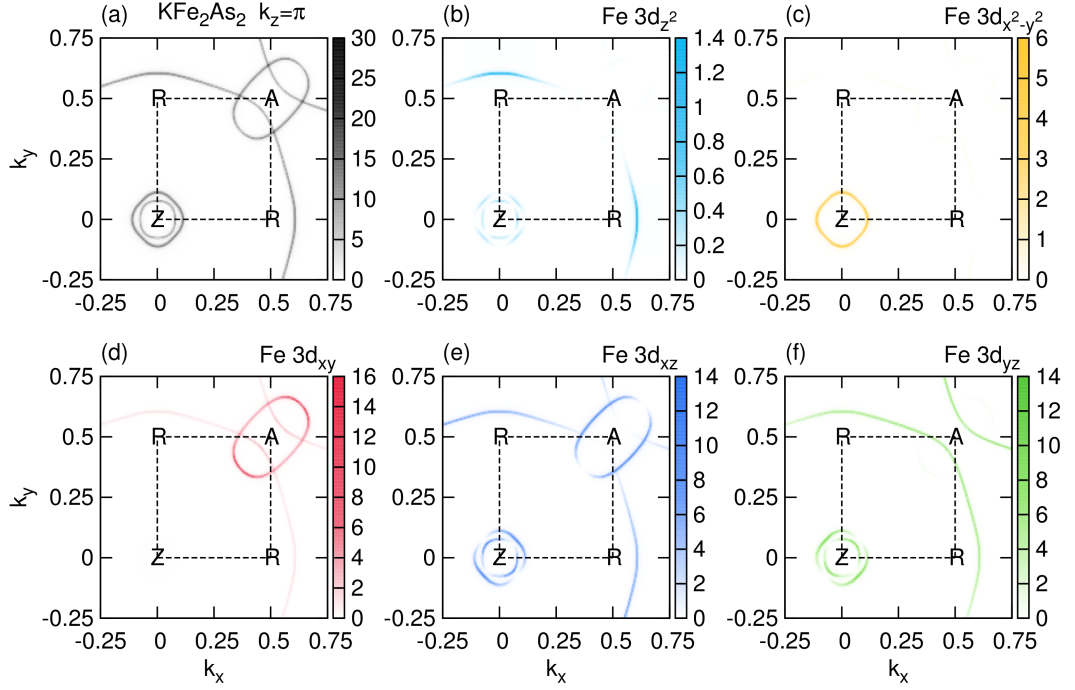


FIG. 8. The $k_z = \pi$ Fermi surface of KFe_2As_2 at $P = 21$ GPa as obtained within LDA+DMFT in the two-Fe Brillouin zone. Panel (a) shows the total spectral function, while panels (b)-(f) show the orbital resolved spectral function for the Fe $3d$ orbitals.